ELSEVIER

Earth and Planetary Science Letters 173 (1999) 439–455

EPSL

www.elsevier.com/locate/epsl

GPS determined eastward Sundaland motion with respect to Eurasia confirmed by earthquakes slip vectors at Sunda and Philippine trenches

N. Chamot-Rooke [a,*], X. Le Pichon [a,b]

[a] *Laboratoire de Géologie, CNRS-URA 8538-1316, Ecole normale supérieure, 24 rue Lhomond, 75231 Paris Cedex 05, France*
[b] *Collège de France, Paris, France*

Received 26 February 1999; revised version received 4 August 1999; accepted 23 September 1999

Abstract

GPS measurements acquired over Southeast Asia in 1994 and 1996 in the framework of the GEODYSSEA program revealed that a large piece of continental lithosphere comprising the Indochina Peninsula, Sunda shelf and part of Indonesia behaves as a rigid 'Sundaland' platelet. A direct adjustment of velocity vectors obtained in a Eurasian frame of reference shows that Sundaland block is rotating clockwise with respect to Eurasia around a pole of rotation located south of Australia. We present here an additional check of Sundaland motion that uses earthquakes slip vectors at Sunda and Philippine trenches. Seven sites of the GEODYSSEA network are close to the trenches and not separated from them by large active faults (two at Sumatra Trench, three at Java Trench and two at the Philippine Trench). The difference between the vector at the station and the adjacent subducting plate vector defines the relative subduction motion and should thus be aligned with the subduction earthquake slip vectors. We first derive a frame-free solution that minimizes the upper plate (or Sundaland) motion. When corrected for Australia–Eurasia and Philippines–Eurasia NUVEL1-A motion, the misfit between GPS and slip vectors azimuths is significant at 95% confidence, indicating that the upper plate does not belong to Eurasia. We then examine the range of solutions compatible with the slip vectors azimuths and conclude that the minimum velocity of Sundaland is a uniform 7–10 mm/a eastward velocity. However, introducing the additional constraint of the fit of the GEODYSSEA sites with the Australian IGS reference ones, or tie with the NTUS Singapore station, leads to a much narrower range of solutions. We conclude that Sundaland has an eastward velocity of about 10 mm/a on its southern boundary increasing to 16–18 mm/a on its northern boundary.

Keywords: Sunda Shelf; movement; Global Positioning System; Southeast Asia; plate tectonics

1. Introduction

The Sundaland block, that includes Indochina (Vietnam, Laos, Cambodia, Thailand and Malaysia), the Sunda shelf, Borneo, Sumatra and Java, is the southeastern extremity of the vast zone of Asia affected by the continental collision between India and Asia (Fig. 1). The absence of significant internal seismicity suggests that the block behaves as a single lithospheric block of a size comparable to the Philippine Sea plate. Because Sundaland is mostly surrounded by subduction boundaries except to the north where a connection with the stable Eurasian plate (Siberia) occurs through a series of deforming and moving blocks, its motion with respect to the

* Corresponding author. Tel.: +33 1 44 32 22 54; Fax: +33 1 44 32 20 00; E-mail: rooke@sphene.ens.fr

0012-821X/99/$ – see front matter
PII: S0012-821X(99)00239-3

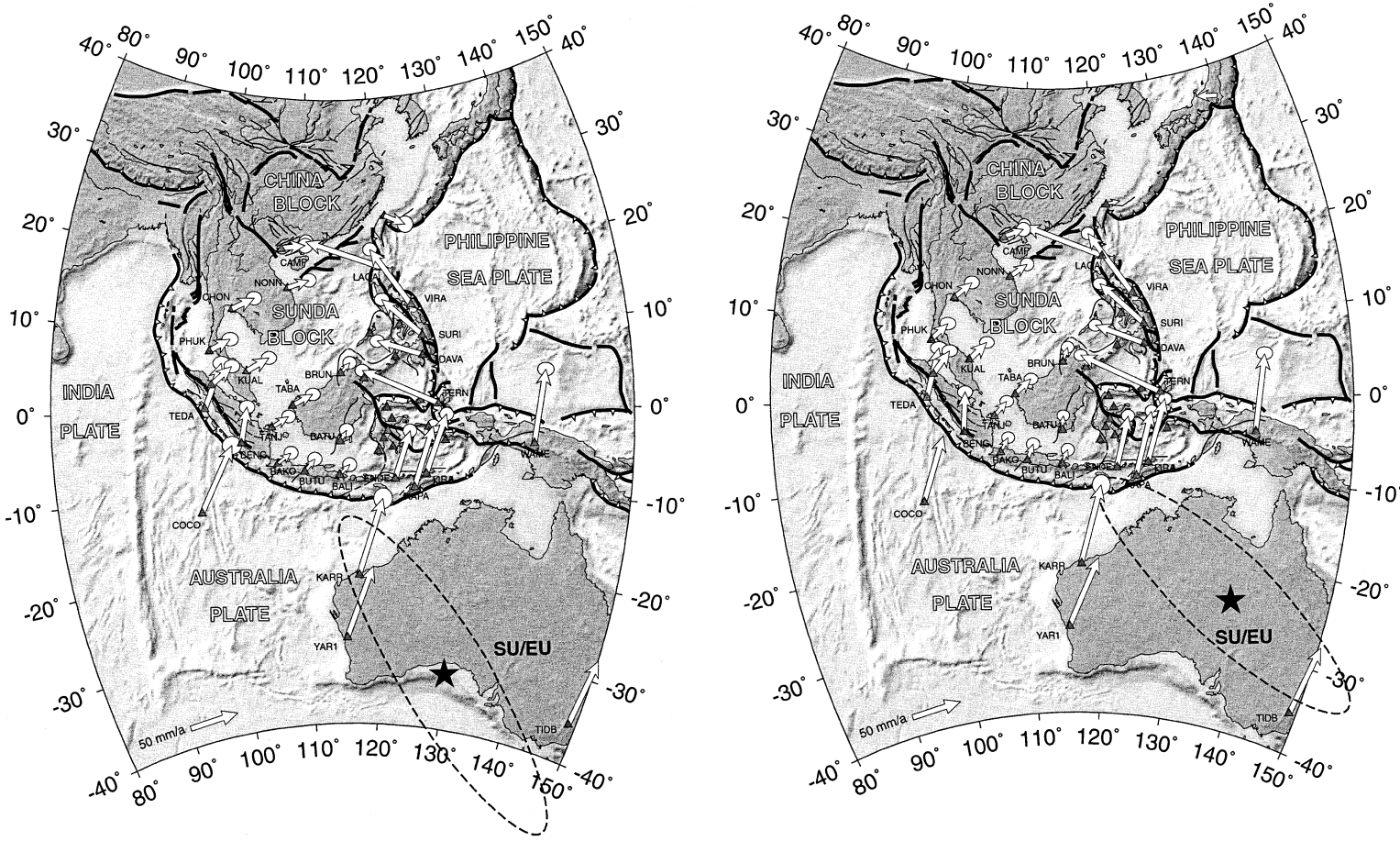

Fig. 1. (Left) Velocity vectors of the GEODYSSEA ITRF-94 solution in a Eurasian reference frame ($3-\sigma$ confidence ellipses) and location of the Sundaland/Eurasia (*SU*/*EU*) pole of rotation with $3-\sigma$ confidence ellipse. The pole was determined using ten stations belonging to rigid Sundaland [13] (from west to east: PHUK, MEDA, CHON, KUAL, TANJ, BAKO, NONN, TABA, BUTU, BALI). Major faults and plates are indicated. For the sake of clarity, some of the GEODYSSEA vectors are omitted. (Right)

surrounding plates remains poorly constrained. Yet, the knowledge of this motion is critical to test the validity of models of continental deformation in Asia. This is demonstrated when comparing the conclusions of three recent kinematic models. Holt et al.'s model has an eastward velocity with respect to stable Eurasia increasing southward from 10 mm/a to the north of South China to about 20 to 30 mm/a to the south [1]. Peltzer and Saucier find a solution where the eastward velocity increases northward from 9 mm/a, to the south of the South China block, to 11 mm/a, to the northeast of it, near Shanghai [2]. England and Molnar finally conclude that South China is moving ESE at less than 10 mm/a and might not be moving at all [3,4].

GPS measurements indicate that sites in eastern Asia are moving east to southeast relative to Eurasia [5–7]. The range of velocities is 9–11 mm/a at Taejon in Korea, 5–9 mm/a at Xian in China, 13–15 mm/a at Wuhan, 11–13 mm/a at Shanghai, 16–18 mm/a at Taipei in Taiwan. The South China block thus appears to rotate counterclockwise, reaching a velocity of 15 to 18 mm/a along its boundary with Sundaland, according to the latest kinematic model [7]. Until recently, no site was available south of China, on the Sundaland block proper. Station NTUS in Singapore is now one of the permanent IGS sites, and preliminary solutions based on 16 to 20 months of measurements are in the range 11–19 mm/a to the northeast to east (14 mm/a to N63º according to Heflin, version 99.5, **http://sideshow.jpl.nasa.gov/mbh/series.html**; other solutions available at **http://bowie.mit.edu**).

Recently, the GEODYSSEA GPS solution based on data from two GPS measurement campaigns at 42 sites over Southeast Asia in December 1994 and April 1996 has established that Sundaland block is non-deformed at the level of precision of GPS measurements [8–10]. For ten stations belonging to this block, the residuals obtained by subtracting a best rigid rotation have r.m.s. below 2.5 mm/a for both the east and north components, indicating very small relative motion for these stations. Mapped into an Eurasia reference frame, Sundaland rotates clockwise around a pole of rotation located south of Australia, with an east to northeast velocity increasing from 14 mm/a to the south to 23 mm/a to the north [10–13] (Fig. 1). The important implications of the motion of Sundaland for the kinematics of South China have been discussed elsewhere [14].

Although the GEODYSSEA network was carefully attached to the ITRF reference frame using IGS stations [10], the use of only two periods of measurements may lead to doubt about the quality of this global attachment and consequently the validity of the derived Sunda/Eurasia (SU/EU) motion. We present here an independent check of the GEODYSSEA global solution reference frame that uses earthquakes slip vectors at trenches and confirms that Sundaland is having a significant motion with respect to Eurasia.

2. Methodology

A difficulty with GPS measurements is to evaluate the reliability of the tie of the network to a rigorous geodetic reference frame. Although the adjustment of the network to a global frame is of less importance when dealing with internal deformation within the network itself, it becomes crucial in plate motion studies. Local GPS networks, in particular, are difficult to tie into a global reference frame. Relative horizontal velocity vectors may be obtained with a very high accuracy, the uncertainties being derived by scaling the formal errors [15,16]. Based on the non-rigid component of motion for the Sundaland block, the accuracy of the relative horizontal velocities of the GEODYSSEA solution is of the order of 3 mm/a. This level is comparable to the formal $(1-\sigma)$ accuracy, which is of 2–3 mm/a for all stations. It was shown further that the relative accuracy remains unchanged for different global computations, in particular different numbers of IGS stations included or different terrestrial reference frames used [10]. A comparison of two global solutions, one obtained in the ITRF-94 reference frame and the other obtained in the ITRF-96 reference frame, shows that although they agree within $3-\sigma$ error values [10], the final SU/EU pole of rotation is strongly influence by the use of different terrestrial frames and the number of IGS sites included.

We use in this paper the fact that subduction zones surround Sundaland to put additional constraints on the global adjustment, using earthquake slip vectors at trenches.

2.1. The kinematic model

The simple kinematics followed in this paper is summarized schematically in Fig. 2. Let us first assume that the velocity vector of the subducting plate (V) is known with respect to a given reference frame R_1. For simplicity, this subduction vector is taken constant along the entire portion of the subduction zone in Fig. 2, but the model does not require it. GPS measurements are available at three stations (A, B and C) close to the subduction edge. We assume that the GPS vectors (V_{GPS}) were obtained in a frame of reference R_2. If R_1 and R_2 are identical, then the difference between the vector at the site and the adjacent subducting plate velocity (or difference vector $V_{SUB} = V_{GPS} - V$) is the relative subduction vector. When mapped into the upper plate or lower plate reference frame, this relative subduction vector is free of any other external frame of reference, and should thus be aligned with the earthquakes slip vectors. We show in Fig. 2a a hypothetical situation where each of the difference vectors does not coincide with the local slip vector azimuth but instead has an angular misfit dα. The conclusion is that R_1 and R_2 are not identical. In other words R_2, the GPS reference frame, has some motion with respect to R_1, the subducting plate velocity reference frame.

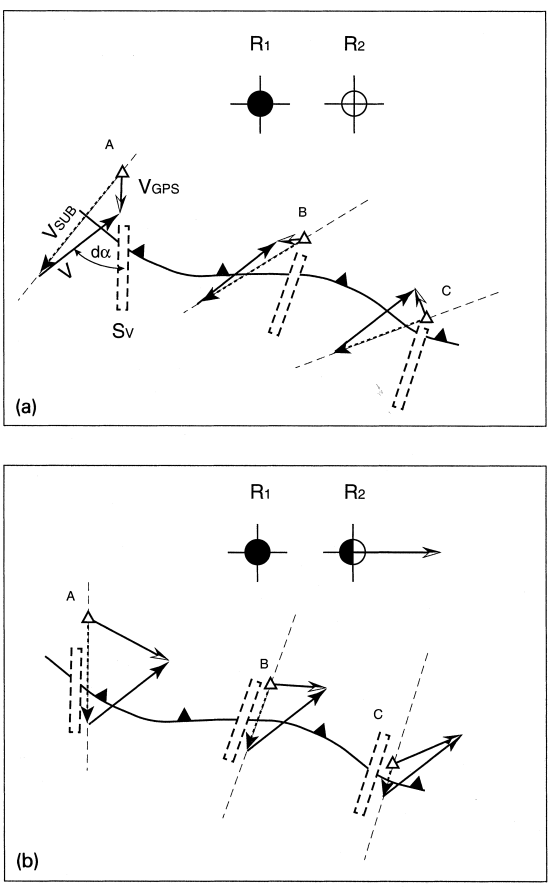

Fig. 2. Kinematic model used in this paper. V is the velocity vector of the subducting plate with respect to a given reference frame R_1 (V is constant along the entire portion of the subduction zone). V_{GPS} is the GPS vector obtained at three stations close to the trench (A, B and C) in a frame of reference R_2. V_{SUB} is the difference vector $V_{GPS} - V$ (subduction vector), which should be aligned with the earthquakes slip vectors (shown as bars) if R_1 and R_2 reference frames are identical. The case shown here is for R_2 having an eastward motion with respect to R_1. (a) Shows the misfit of the predicted slip versus observed slip if the motion of R_2 with respect to R_1 is not included, dα is the misfit angle. (b) Shows that the misfit drops to zero if the motion of R_2 with respect to R_1 is included.

The next step is shown in Fig. 2b: using the same GPS network solution, the angular misfit dα drops to zero at each of the three stations if we allow for a whole motion of the GPS network (taken here due east and constant for simplicity). Notice that if we use a single GPS station, then the motion of R_2 with respect to R_1 is not unique since a full range of motion would actually bring the expected slip on the observed slip. If several stations are used, the motion of R_2 with respect to R_1 can be obtained by minimizing the angular misfits dα. In a later section of the paper, we show that one can also proceed by exclusion to retrieve the range of acceptable solutions given the errors on the slip vector azimuths, the GPS vectors and plate motion vectors. On a sphere, the reference frame adjustment will simply be a rigid rotation.

The slip vector azimuths can thus be used as additional constraints to test the adequation of the reference frame. The angular misfits contain some information on the consistency of the subducting plate velocity reference frame and the GPS vectors reference frame.

2.2. Transient seismic effects

The methodology described above does not require the upper plate to be rigid: it is obviously deforming

in the example shown in Fig. 2. The final motion which is obtained describes reference frames motion, not plate motions. However, a requirement of the method is that the GPS motion at sites used is identical to the plate edge motion. This implies that there should be no deformation (either permanent or transient) between the site and the edge of the plate. Thus, any shear partitioning, such as in Sumatra and Philippine trenches, should be located landward of the sites used. In addition, these sites should be located at some distance from the faults to avoid elastic loading effects on locked segments.

The subduction plane may be locked during the interseismic phase, thus producing elastic deformation of the upper plate that affects the difference vectors obtained as described above. The Sumatra subduction zone appears to be locked now [13,17] and the Philippine subduction zone is probably locked too [18]. The Java subduction zone seemed to be unlocked based on the low level of seismicity in recent time [13,19,20]. However, following a relative quiescence of seismic activity along the central portion of the Java Trench, a large earthquake of magnitude 7.8 occurred on June 2, 1994 off Bali [21]. Such a large seismicity release may be difficult to reconcile with the early hypothesis of an unlocked subduction zone there.

We thus need to investigate the possible perturbations introduced by the effect of elastic coupling on the subduction plane. If the subduction vector is perpendicular to the subduction zone, the elastic loading vector is parallel to the subduction vector everywhere and consequently does not produce any deviation of the difference vector from the actual subduction one. This is the case along the Java Trench, and the effects of coupling can thus be ignored there.

If however, the subduction vector is oblique to the trench, as is the case along the Sumatra Trench, and less so, along the Philippine Trench, the difference vector is systematically affected by a deviation of azimuth. This deviation is particularly large for

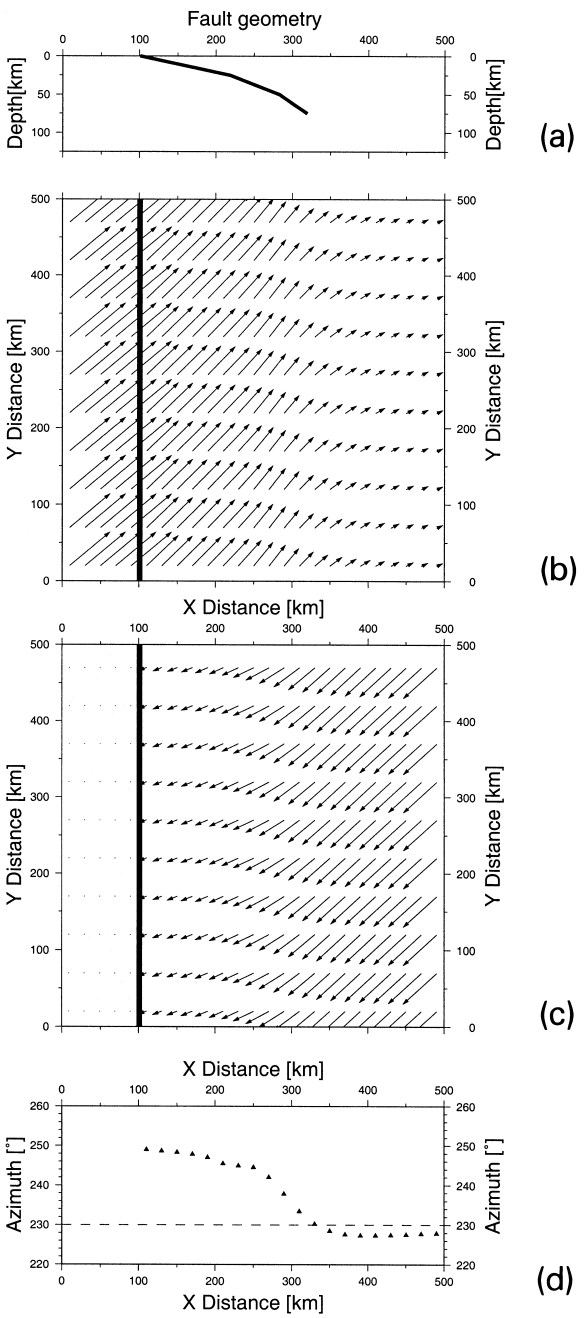

Fig. 3. Interseismic elastic loading along the locked portion of a subduction plane, assuming a 40° obliquity of the subduction vector. (a) Geometry of the locked plane for the Sumatra Trench (after [17]). (b) Modeled velocity field with respect to a stable upper plate away from the elastic coupling zone. (c) The same velocity field recalled in a subducting plate reference frame (the subducting plate velocity vector has been subtracted). (d) The expected azimuth of the velocity vectors, compared to the azimuth of slip (230°). The deviation is small away from the locked zone only.

stations that would be situated above the locked portion of the subduction zone. To quantify this effect, we model the elastic coupling for a slab geometry (Fig. 3a) that closely resembles the Sumatra subduction zone [17]. The interseismic elastic loading phase is described by a combination of a steady state slip along the fault surface (reverse motion) and an opposite direction dislocation (normal motion) along the locked portion of the fault [22]. The elastic coupling effect is shown in Fig. 3b in an upper plate reference frame, and in Fig. 3c in a subducting plate reference frame. In the latter frame, the obtained vectors can be directly compared to the subduction vector. Away from the locked zone (distance greater than 300 km in this example), the vector azimuth is aligned with the slip vector azimuth (230º) within 2º (Fig. 3d). Above the locked zone, the 40º obliquity of the subduction direction produces a clockwise deviation of up to 20º. In addition, the difference vector there is small and consequently, it cannot be used simply to obtain the direction of subduction. We thus conclude that stations located above the coupling plane are inadequate but that these located landward of the coupling plane can be used.

3. Is Sundaland moving with respect to Eurasia?

3.1. Sites selection

Seven sites of the GEODYSSEA network are close to the trenches and not separated from them by large active faults. Two sites at the Sumatra Trench (BENG and TEDA) and three sites at the Java Trench (BALI, BUTU and BAKO) are related to subduction of the Australian plate below Sundaland (AU/SU). Two sites at the Philippine Trench (VIRA and SURI) are related to the subduction of the Philippine Sea plate below Sundaland (PH/SU) (Fig. 4 and Table 1). Some other sites of the GEODYSSEA network are also close to a trench, but they were rejected for different reasons. Stations at the eastern end of the Java Trench (ENDE, KAPA and LIRA) are located in the complex area of collision with Australia [23]. Some other sites are separated from the trench by active faults (TAIW in Taiwan, LAOA in northern Luzon, DAVA in Mindanao) and cannot be used further [18]. The GEODYSSEA GPS vectors, referred to Sundaland using a solution that minimizes motions of ten sites situated on non-deformed Sundaland [13] are shown in Fig. 4a. Velocity vectors for the selected sites discussed in this paper are listed in Table 1. We use the official GEODYSSEA solution mapped into ITRF-94, although an ITRF-96 solution is also available now. Remapped into a Sundaland reference frame, we checked that both solutions are similar for the seven stations we are using here (see [10] for further details on both solutions).

Transient elastic effects may affect some of the selected sites. Site TEDA off Sumatra is the only site that is located above the locked subduction plane. The consequence is that elastic deviation may be large and that the difference vector may be small, so that this site cannot be used to obtain the subduction vector direction. However, site TEDA still gives a constraint for Sundaland motion as it is required that the solution results in subduction there. This constraint will be used in a further section of this paper.

Another possible transient effect may come from the proximity of sites BENG (Sumatra) and SURI (Philippines) to large active strike-slip faults. Site SURI is situated only 15 km away from the Philippine Fault with a rate of left-lateral slip of 27 ± 7 mm/a to 337º [18]. The seismogenic zone appears to be 15 km thick along this fault [24]. Using the standard arctangent velocity distribution across an infinitely long strike-slip fault [25], the maximum transient effect would be 7 ± 2 mm/a there. However, two recent detailed geodetic surveys on this fault indicate that it is unlocked at the present time further north [26,27], near 11ºN and 12.5ºN and the fault may also be unlocked at SURI, one degree further south, although we have no further data to argue for coupling or uncoupling there.

Based on a very detailed GPS network, the northern segment of the Great Sumatra Fault (GSF) is locked [17]. From the same data set, the Mentawai fault, a possibly active strike-slip fault across the fore-arc [28], does not show in the GPS measurements. The southern GSF is less well known. Site BENG is located 45 km away from one of the southern segments of the GSF. The long-term rate of slip on this portion of the fault is estimated to be 11 ± 5 mm/a based on geomorphic offsets [29]. Assuming that this segment of the fault is locked, and adopting

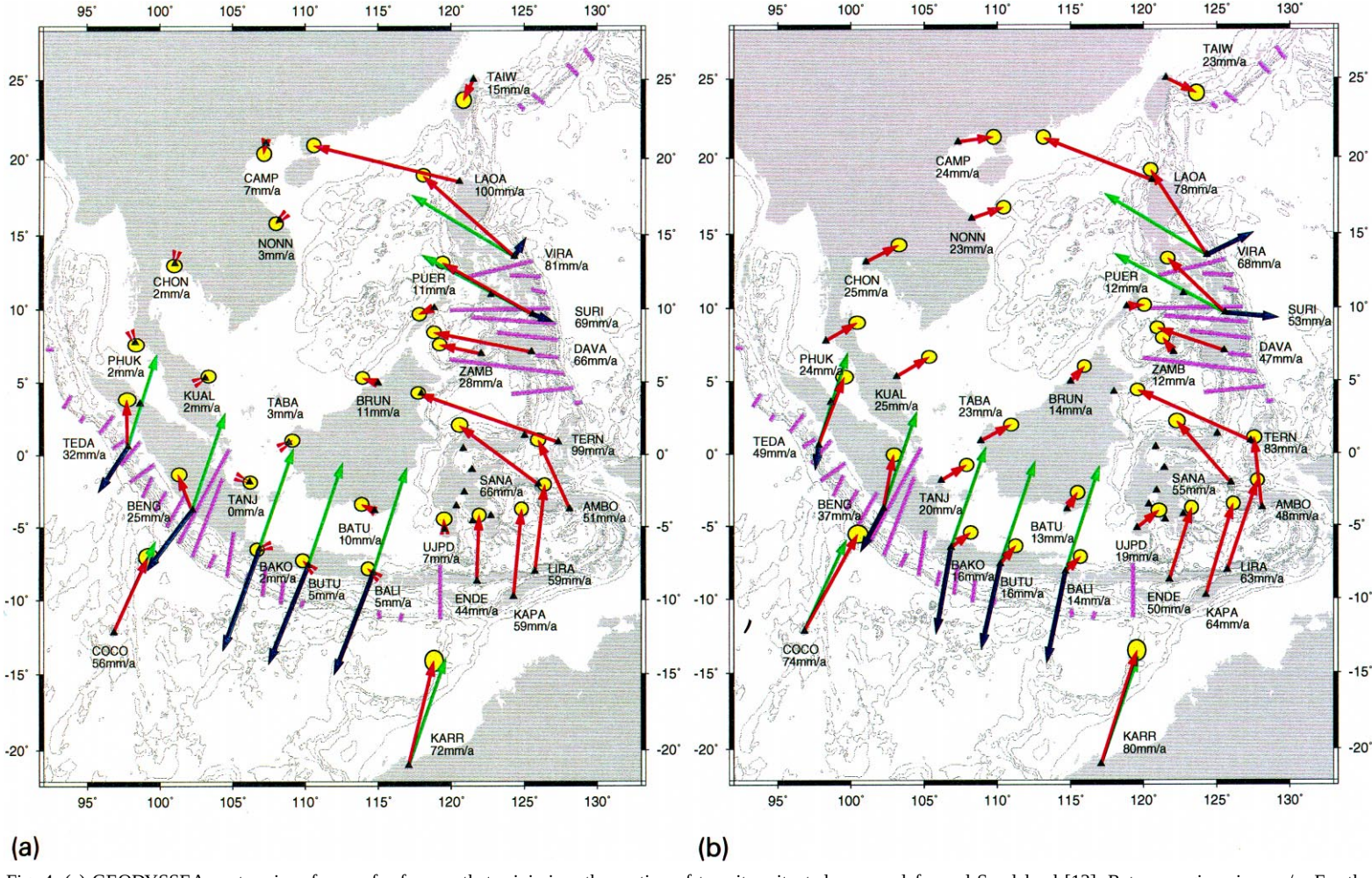

Fig. 4. (a) GEODYSSEA vectors in a frame of reference that minimizes the motion of ten sites situated on non-deformed Sundaland [13]. Rates are given in mm/a. For the sake of clarity, some of the GEODYSSEA stations are omitted. Ellipses are 95% confidence intervals. Green vectors are the subducting plate velocity vectors derived from PH/EU and AU/EU NUVEL1-A model. Blue vectors are the difference vectors (GEODYSSEA minus subducting plate velocity vector), which should be aligned with the earthquakes slip vectors if the reference frames were identical. The slip azimuths are shown as purple bars, the length of each bar being inversely proportional to the number of earthquakes used to determine it. (b) The same as (a) except that the GEODYSSEA vectors are taken from the global solution obtained in a Eurasian reference frame.

Table 1
GEODYSSEA GPS vectors in a Sundaland frame of reference (Veast, Vnorth, azimuth, velocity) and NUVEL1-A predictions for the subduction vectors (azimuth, velocity)

	Lat. (°N)	Lon. (°E)	Veast (mm/a)	Vnorth (mm/a)	GEODYSSEA		NUVEL1-A	
					Azim. (°)	Velocity (mm/a)	Azim. (°)	Velocity (mm/a)
Stations facing the Philippine Sea plate								
VIRA [a]	13.57	124.34	−60.6 ± 2.3	54.2 ± 2.2	312	81.3	301	80.0
SURI [a]	9.65	125.58	−59.8 ± 2.4	34.8 ± 2.1	300	69.2	298	84.0
Stations facing the Australia plate								
BALI [b]	−8.15	114.68	−3.6 ± 2.3	2.9 ± 2.3	309	4.6	18	74.6
BUTU [b]	−7.64	110.21	−3.5 ± 2.3	3.2 ± 2.2	313	4.8	18	73.0
BAKO [b]	−6.49	106.85	−1.4 ± 2.4	−0.5 ± 2.2	252	1.5	19	71.5
BENG [b]	−3.79	102.25	−9.0 ± 2.6	23.7 ± 2.3	339	25.4	19	68.8
TEDA [b]	0.57	97.82	−0.4 ± 2.9	31.8 ± 2.3	359	31.8	17	65.2
Stations belonging to the Australia plate								
COCO [b]	−12.19	96.83	23.3 ± 3.3	50.5 ± 3.0	25	55.6	25	67.6
YAR1 [b]	−29.05	115.35	24.0 ± 0.0	64.1 ± 0.0	21	68.5	21	76.1
KARR [b]	−20.98	117.10	16.9 ± 3.1	70.1 ± 3.5	14	72.1	19	76.0
TIDB [b]	−35.40	148.98	6.9 ± 0.0	78.3 ± 0.0	5	78.6	2	70.1
Station at the boundary between South China and Sundaland								
CAMP	21.00	107.31	−1.2 ± 2.5	−6.9 ± 2.4	190	7.0		

[a] Philippines Sea plate.
[b] Australia plate.

an upper bound estimate of 19 mm/a of right-lateral strike slip motion [13], the maximum expected transient at site BENG would be less than 2 mm/a.

We have systematically tested the effects of these two transients (proximity to the locked subduction plane, proximity to the transcurrent faults). The effect increases as the magnitude of the difference vector decreases. We have found that when we assume that Sundaland belongs to Eurasia the corrections to the azimuths are less than the $1-\sigma$ error on the slip vectors and can be ignored for all cases except one: site SURI. In that only case the corrections on the derived subduction vector is large because the vector magnitude is small.

3.2. The slip vectors test at Sumatra, Java and Philippine trenches

We first assume that Sundaland is part of Eurasia, and consequently that the GPS reference frame of Fig. 4a is actually a Eurasian reference frame. This is exactly equivalent to assuming that R_2 (Sundaland reference frame) is identical to R_1 (Eurasian reference frame) in our theoretical example of Fig. 2. We call it the slip vectors test, since slip vector azimuths contain the information on the compatibility of R_1 and R_2. The subducting plate velocities in a Eurasian frame of reference were derived from the PH/EU and AU/EU vectors given respectively by

Table 2
Plate pairs rotation parameters used in this study

Plate pair	Rotation parameters			Standard error ellipse				Reference
	Lat. (°N)	Lon. (°E)	ω (°/Ma)	σ_{max} (°)	σ_{min} (°)	ζ_{max} (°)	σ_w (°/Ma)	
SU/EU	−33.23	129.83	−0.286	7.9	1.8	−38	0.03	[13]
AU/EU	15.11	40.45	0.688	2.1	1.1	−45	0.01	Nuvel1-A [31,32]
PH/EU	48.23	156.97	−1.038	2.8	0.7	56	0.07	Seno recalibrated [30]

AU = Australia plate; SU = Sundaland plate; EU = Eurasia plate; PH = Philippines Sea plate.

Table 3
Slip vectors azimuths

	N	Azimuth (°)	Reference
VIRA	9	256 ± 8	[34] PH01
SURI	13	269 ± 12	[34] PH04
BALI	7	5 ± 4	[13]
BUTU	3	13 ± 8	[13]
BAKO	14	11 ± 6	[13]
BENG	22	29 ± 14	[34] JS11/12/13

N = number of earthquakes, error = $1-\sigma$.

Seno et al. [30] and DeMets et al. [31,32] (see Table 2). Although the PH/EU kinematics have been more difficult to establish, because the Philippine Sea plate is surrounded by subduction zones, recent geodetic measurements within this plate [18,33] confirm that Seno's model is essentially correct. We have however modified the error ellipse of Seno to take into account these new direct measurements of the Philippine Sea plate motion. The difference vectors were derived for the six sites, and their azimuths systematically compared with the azimuths of the slip vectors using statistics on slip vectors of subduction earthquakes (Table 3, after [13,34]). We used here the conventional way of estimating the slip vectors azimuths and associated errors, which is based on a population of selected thrust earthquakes and calculation of mean azimuth and standard deviation. The use of Gaussian statistics of this type may not be appropriate for slip vectors, and we will use a more realistic method in a further section of the paper. At this stage, these statistics are accurate enough to demonstrate that Sundaland is having significant motion with respect to Eurasia.

Fig. 4a (detailed in Fig. 5a for Sunda trenches and Fig. 6a for the Philippine Trench) and Table 4 compare the solution with Sundaland being part of Eurasia (IV-1) and the solution with Sundaland having the motion inferred from GEODYSSEA (IV-2). The standard deviation (using circular statistics on the misfit) is 27° for the solution with no motion of Sundaland and drops to 8° if Sundaland motion is included. Although as stated above the data we use may not follow the underlying assumptions of standard statistics, application of an F-ratio test [35,36] indicates that the introduction of an additional plate (Sundaland) improves the fit at a confidence level of 95%. The error on the azimuth of the difference vector being inversely proportional to the magnitude of the vector, the misfit may be strongly influence by small variations of the GPS vector and plate motion vectors. This will be particularly true for stations VIRA and SURI in the case of no motion of Sundaland: the magnitude of the difference vector there is only 15 mm/a, and varying the GEODYSSEA GPS vectors and the predicted Nuvel-1A vectors into their respective $1-\sigma$ error ellipses leads to 18° and 14° of error at VIRA and SURI. To quantify this effect, we allowed the GPS and Nuvel-1A vectors to fluctuate into their $1-\sigma$ error ellipses and determined the difference vector which best fit in azimuth the mean slip vector. With no motion of Sundaland, we still find a significant misfit at all sites, including VIRA and SURI. If Sundaland motion is included, the same calculations give a misfit of less than one degree at four sites. The F-ratio test becomes positive at a confidence level of 98%.

The discrepancy between slip vectors and predicted subduction motion between Eurasia and Aus-

Table 4
Difference vectors and angular misfit with the observed subduction azimuth. (1) Solution with no motion of Sundaland. (2) Solution with Sundaland motion derived from Chamot-Rooke et al. [13]

	Observed (°)	(1)			(2)		
		Velocity (mm/a)	Azimuth (°)	Misfit (°)	Velocity (mm/a)	Azimuth (°)	Misfit (°)
VIRA	256	15	212 ± 18	−44	35	244 ± 7	−12
SURI	269	15	291 ± 14	22	36	275 ± 6	6
BALI	5	73	21 ± 3	16	62	12 ± 3	7
BUTU	13	71	22 ± 3	9	59	13 ± 4	0
BAKO	11	72	20 ± 3	9	59	10 ± 4	−1
BENG	29	52	37 ± 4	8	33	28 ± 7	−1

Error = $1-\sigma$.

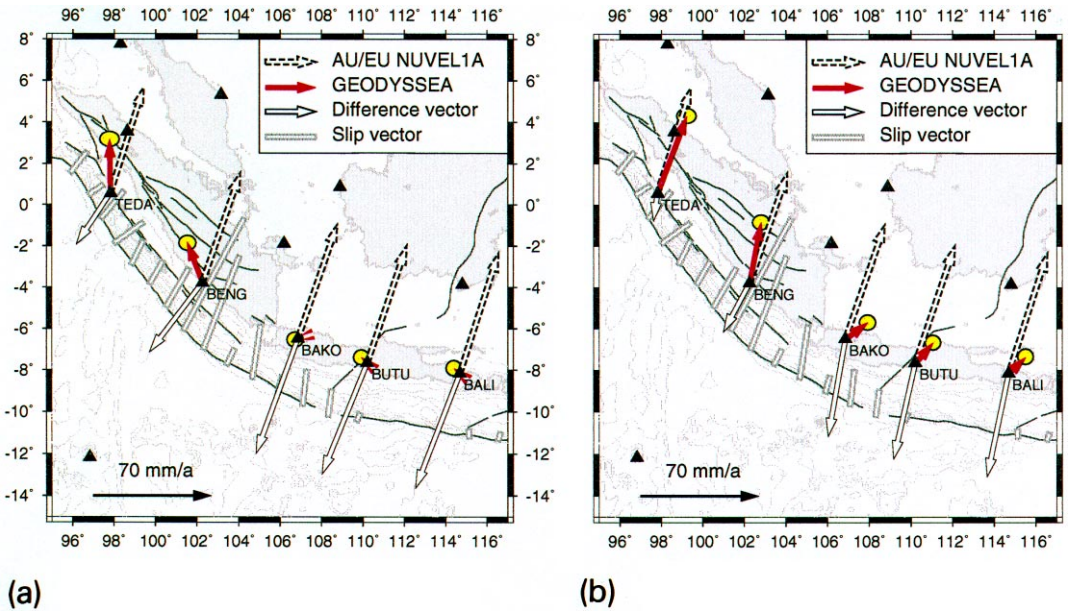

Fig. 5. Details of Fig. 4 in the area of Sunda trenches, with major faults added. Color code is as in Fig. 4. (a) Solution obtained assuming no Sundaland motion with respect to Eurasia (same as Fig. 4a). (b) Solution obtained using GEODYSSEA vectors from the global solution in a Eurasian reference frame (same as Fig. 4b).

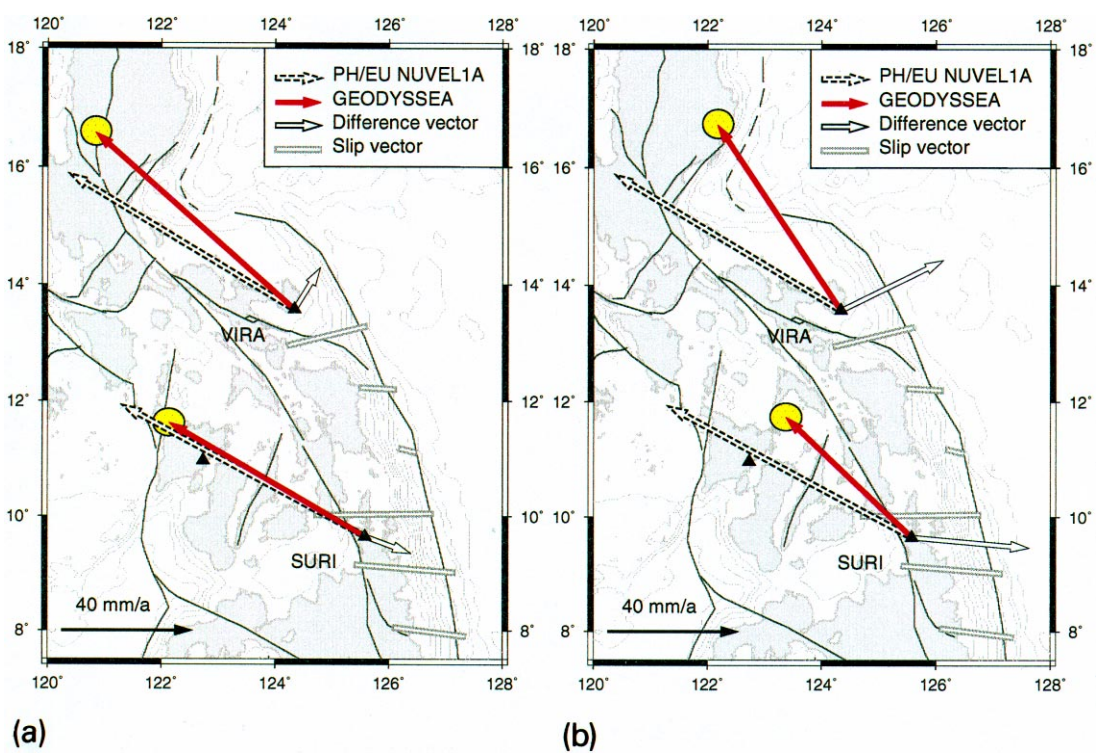

Fig. 6. Details of Fig. 4 in the area of the Philippine Trench, with major faults added. Color code is as in Fig. 4. (a) Solution obtained assuming no Sundaland motion with respect to Eurasia (same as Fig. 4a). (b) Solution obtained using GEODYSSEA vectors from the global solution in a Eurasian reference frame (same as Fig. 4b).

tralia at Java Trench has long been recognized [37] and is now confirmed by GPS measurements [13,21]. This incompatibility between Sundaland being part of Eurasia and directions of slip vectors at trenches is thus well established for the Java Trench. We confirm here that the same type of incompatibility exists at the Philippine Trench [18]. The slip vectors test thus demonstrates that at a confidence level greater than 95%, Sundaland is having a significant motion with respect to Eurasia. Although the GEODYSSEA global solution is clearly compatible with the slip vectors at Sunda and Philippine trenches, this solution may not be unique. The next step is to explore the possible range of motions of Sundaland with respect to Eurasia that would still be compatible with the slip vectors at trenches.

4. Range of Sundaland motions with respect to Eurasia that are compatible with the subduction slip vectors

4.1. Motion obtained from slip vectors only

We proceed by systematic exploration of the model space and exclusion [38]. The systematic exploration (rather than a random or Monte Carlo exploration) is made possible by the small number of parameters to search for (three for a pole of rotation). Rather than using mean slip vectors estimates and associated Gaussian statistics (square root of the variance) at various sites, we use a more rigorous approach by introducing all slip vectors into the inversion. The rationale is to optimize the inversion by taking into account individual errors on slip vectors. The Harward CMT catalog contains the uncertainties for each of the moment tensor components. Following Frohlich and Davies [39], an estimate of the errors on various parameters, including slip vectors, can be obtained by varying each of the six elements of the moment tensors into their $1-\sigma$ error ellipses. For each of the selected earthquake, we formed the 15,625 (or 5^6) moment tensors and recalculated the slip vector. An estimation of the error on the azimuth slip vector was taken as the maximum deviation obtained among the 15,625 moment tensors set. Before this procedure, strict selection criteria were used to eliminate inappropriate datum: earthquake with strong non-dipole components, or with large errors to moment components ratio, or with some of the moment tensor elements indeterminate [39]. Forty earthquakes were retained, equally distributed between the Philippine side (15 around VIRA and SURI), Sumatra side (14 around BENG) and Java side (11 around BAKO, BUTU and BALI).

We thus explore systematically the full range of solutions for the SU/EU rotation vectors, and test at each individual site the misfit between the azimuth of the difference vector and the slip vectors azimuth ($d\alpha$ in the theoretical example of Fig. 2). Three different sources of errors are introduced: errors on the GPS vectors, errors on the Nuvel-1A plate motion vectors, errors on the azimuth of slip vectors. If for any of the 40 slip vectors data $d\alpha$ is larger than some pre-defined confidence interval, taking into account the error on the difference vector with the same confidence interval, then the solution is excluded. The zones where the possible poles of rotation are located are shown in Fig. 7a. The limits of the possible zones correspond to portions of great circles related each to a given site. Site TEDA is used as an additional constraint to retain solutions that give subduction there, but the misfit azimuth at this site is not used further as explained previously.

The best location for the SU/EU pole of rotation obtained solely from slip vectors is slightly north of the GEODYSSEA solution, put predicts unrealistic high velocities. Further, this new solution does not improve significantly the slip vectors azimuths fit compared to the GEODYSSEA solution. Actually, poles located into the 80% confidence region fit equally well the slip vectors constraints. The GEODYSSEA pole obtained from the ITRF-94 solution is inside the 80% confidence interval, whereas the pole obtained from the ITRF-96 solution is outside the 80% confidence interval but inside the 95% confidence interval. The reason is that in the latter solution, the east component at Java is too small to deviate slip vectors to their observed values there.

Fig. 8a shows the actual possible ranges of values for the SU/EU vectors at the different sites. At 80% confidence level, the minimum motion solution is a uniform N80° motion of Sundaland, with rates of 10 mm/a at Java increasing to 12 mm/a to the north (station CAMP). At 85% and 90% confidence interval, the minimum motion is uniform towards N100°

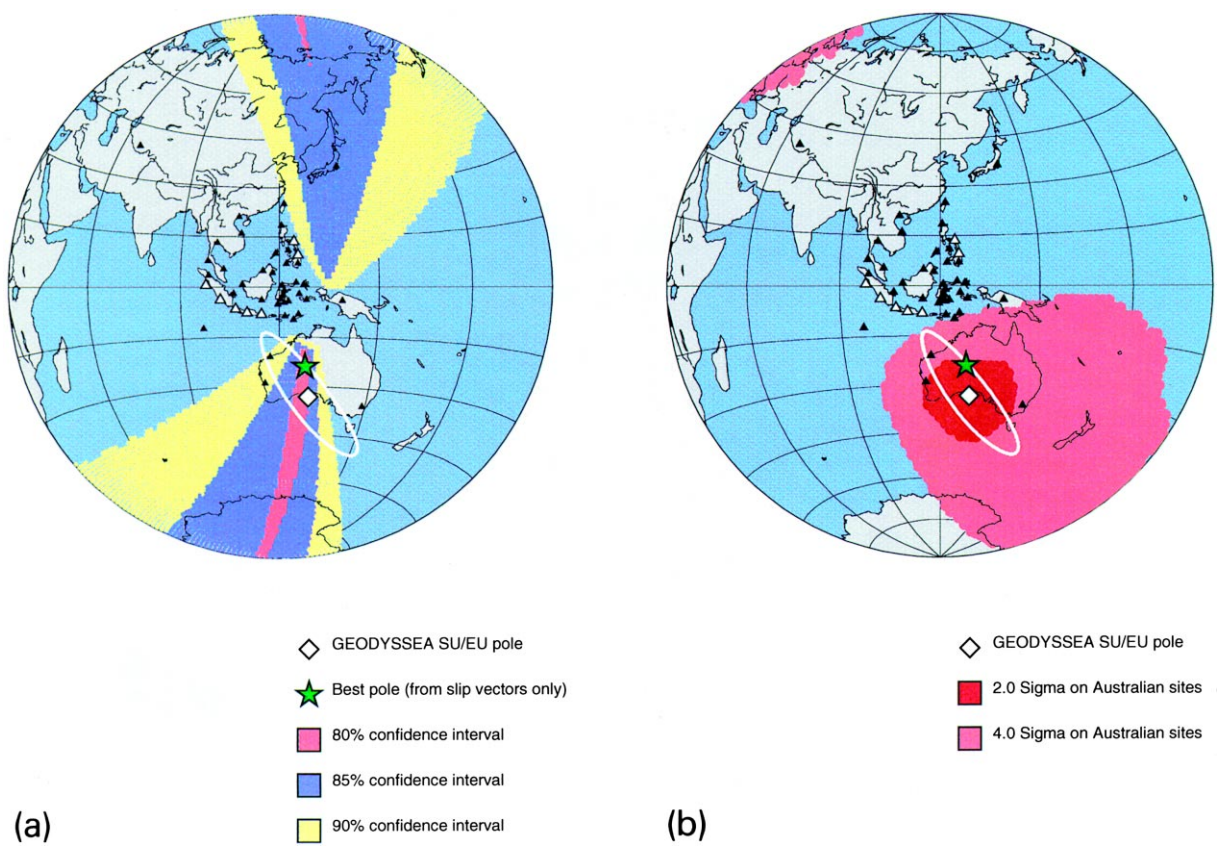

Fig. 7. (a) Range of possible pole locations for Sundaland with respect to Eurasia, obtained by an exclusion model. The misfit between the azimuth of the difference vector and the slip vectors azimuth is examined at each individual site, taking into account errors on the GPS vectors, on the plate motion vectors, and on the individual slip data (40 slip data are used). Regions sampled correspond to 80, 85 and 90% confidence intervals. SU/EU best pole of rotation for this run (green star) is compared with previous determination (diamond, after [13], pole with $3-\sigma$ confidence ellipse). (b) Range of possible pole location compatible within $4-\sigma$ (light red) and $2-\sigma$ (dark red) errors at the Australian GEODYSSEA sites. Other symbols as in (a).

with rates of 7 and 5 mm/a respectively. In the latter case, the fit degrades significantly for the Philippine sites. At 95% confidence interval on all parameters, the solution with no motion of Sundaland is still not retained. We conclude that, independently of any global attachment of the GEODYSSEA geodetic network, the constraints related to the directions of the subduction vectors based on earthquakes slip vectors indicate that Sundaland has a minimum eastward motion of 7–10 mm/a with respect to Eurasia.

4.2. Ties with Australian sites

However, among the solutions that fit the slip vectors at trenches, a large set does not fit the geodetic ties with the global IGS network. In particular, the geodetic ties with the relatively close Australian sites provide important constraints. Fig. 7b shows the range of acceptable pole locations that would not violate the Australian constraints at sites COCO, YAR1, KARR and TIDB (see locations and values in Table 1), within the errors given by the GEODYSSEA solution. For YAR1 and TIDB that were fixed to their ITRF-94 vectors in the GEODYSSEA solution, we have assumed that the errors there are identical to those at KARR (3.5 mm/a for the east and the north component). Australian vectors are first derived into the Sundaland-fixed frame, and we then span the range of SU/EU poles that will bring the Australian vectors into the

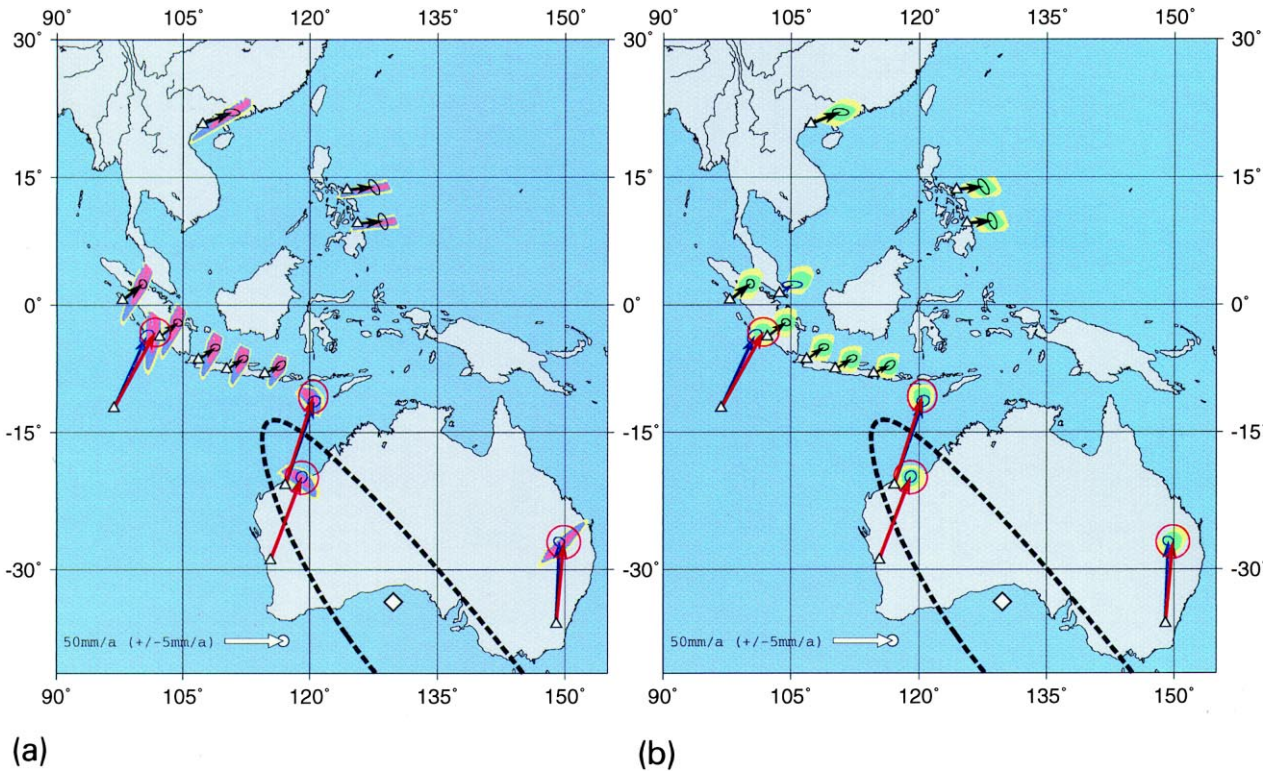

Fig. 8. (a) Range of possible SU/EU vectors predicted at each individual site from the range of possible poles shown in Fig. 7a (slip vectors azimuths constraints only). Notice that these are the correction vectors that bring vectors in the Sundaland frame to vectors in the Eurasia frame. They do represent true velocity vectors with respect to Eurasia only for stations that do belong to Sundaland. The 80, 85 and 90% confidence intervals are shown. For the six upper plate stations discussed in the text, plus TEDA and CAMP, we also show the motion predicted by the SU/EU pole obtained directly from the GEODYSSEA solution (diamond pole, with $3-\sigma$ error ellipse). For the four Australian stations, we show the GEODYSSEA Eurasia-fixed solution (red arrows, with $4-\sigma$ error ellipses) and the NUVEL1-A predictions (blue arrows, $4-\sigma$ error ellipses). (b) Range of possible SU/EU vectors predicted at each individual site from the range of possible poles shown in Fig. 9a (slip vectors azimuths constraints and Australian tie constraints). We show the solution for 95% on the slip vectors and $2-\sigma$ on the Australian sites (green) and the solution for 95% on the slip vectors and $4-\sigma$ on the Australian sites (yellow). The confidence interval for GPS vectors and plate motion vectors is 95% for both runs. Added to this plot is the prediction for site NTUS, together with Heflin's solution there (blue arrow at Singapore, $4-\sigma$ error ellipse). Other symbols are as in (a).

GEODYSSEA Eurasian frame solution. We explored a realistic $2-\sigma$ solution and a conservative $4-\sigma$ solution (Fig. 7b). It appears that many of the poles found from the slip vectors only are incompatible with the Australian constraints. A comparison of Fig. 7a and Fig. 7b shows that the northernmost poles of Fig. 7a can be excluded: this rules out the possibility of having a counterclockwise rotation of Sundaland with respect to Eurasia. Poles that gave the minimum motion of Sundaland in the previous strategy are outside the acceptable range inferred from Australian constraints.

4.3. Motion obtained from slip vectors and Australian constraints

We now combine constraints on the slip vectors with constraints on the Australian sites. The new range of possible poles is shown in Fig. 9a and the corresponding vectors are shown in Fig. 8b. The GPS and plate motion vectors are constrained to their $2-\sigma$ error ellipses, and the slip vectors to their 95% confidence interval. As in the previous section, we test a $2-\sigma$ solution and a $4-\sigma$ solution for the Australian ties. The minimum Sundaland motion for the conservative $4-\sigma$ solution is 4 mm/a to 64° in the south

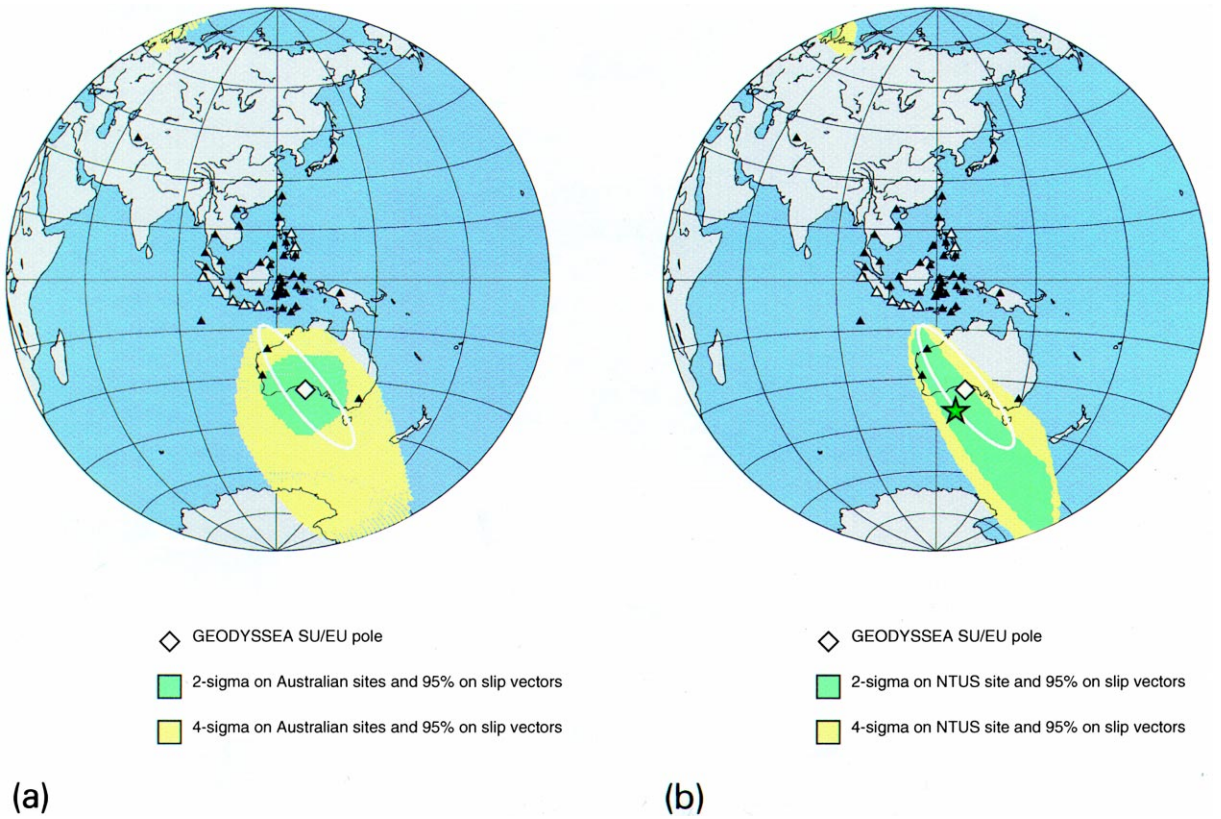

Fig. 9. (a) Range of possible pole locations for Sundaland with respect to Eurasia, obtained by combining slip vectors azimuths constraints and Australian ties constraints. We show the solution for 95% confidence interval on the slip vectors, GPS vectors and plate motion vectors and $2-\sigma$ on the Australian sites (green) and the solution for 95% on the slip vectors, GPS vectors and plate motion vectors and $4-\sigma$ on the Australian sites (yellow) (see the corresponding vectors with same color code in Fig. 8b). Other symbols are as in Fig. 7. (b) Range of possible pole locations for Sundaland with respect to Eurasia, obtained by combining slip vectors azimuths constraints and NTUS site constraint. We show the solution for 95% confidence interval on the slip vectors, GPS vectors and plate motion vectors and $2-\sigma$ on the motion of NTUS (green) and the solution for 95% on the slip vectors, GPS vectors and plate motion vectors and $4-\sigma$ on the motion of NTUS (yellow). The green star locates the best pole. Other symbols are as in Fig. 7.

(Java) and 6 mm/a to 56° on the southern border of South China (site CAMP). For the $2-\sigma$ solution, the rates increase to 10 mm/a towards 60° at Java and 16 mm/a towards 62° at site CAMP. However, in the $4-\sigma$ solution, the predicted vectors at Australian sites are outside the $4-\sigma$ NUVEL1-A error ellipses. This is unlikely since global models indicate no significant differences for the Australia plate between the NUVEL1-A predictions and the GPS determined motion at the 95% confidence limit [40]. Thus, the $4-\sigma$ solution appears to be incompatible with our present knowledge of Australia motion, unless the GEODYSSEA solution is highly distorted.

4.4. Motion obtained from slip vectors and NTUS constraint

A single IGS permanent site is now available to test the motion of Sundaland: station NTUS in Singapore. The latest solution reported by Heflin for this station (solution 99.5) is 14 mm/a, azimuth 63°, with $1-\sigma$ errors of about 0.5 and 1.25 mm/a for the north and east component respectively. This velocity is about 8 mm/a slower than the velocity predicted by the GEODYSSEA SU/EU pole (21 mm/a to the 57°). To free our solution from strong ties of the GEODYSSEA to a global frame, we tested a last type of models in which we derive the SU/EU

poles from constraints on slip vectors together with the NTUS site constraint. Again, the GPS and plate motion vectors are constrained to their $2-\sigma$ error ellipses, and the slip vectors to their 95% confidence interval. We allow $2-\sigma$ to $4-\sigma$ errors on the motion of site NTUS. The range of solution is shown in Fig. 9b. For both solutions, the minimum Sundaland motion is about 10 mm/a to the N60º. The best pole is located at S39.95º/E127.08º with a rotation rate of −0.178º/Ma. It fits GEODYSSEA Australian ties within $2-\sigma$ and predicts a motion of Java with respect to Eurasia of about 11 to 12 mm/a towards N65º–N70º, increasing to 18 mm/a towards N73º at station CAMP. The difference between this best solution and GEODYSSEA solution is a decrease of the GEODYSSEA velocities of about 4 to 5 mm/a for southern Sundaland, and of about 8 to 9 mm/a for the northern part of Sundaland. The predicted vectors are within the $3-\sigma$ error ellipses obtained by GEODYSSEA (global frame solution), equivalent to the global accuracy quoted previously [10].

5. Conclusion

Using the slip vectors as an additional constraint, we show that Sundaland does not belong to Eurasia but has an east to east-northeast velocity that is larger than 7–10 mm/a, even if one ignores the ties with the Australian stations. Actually, these ties prevent any solution in which the velocity of Sundaland with respect to Eurasia is less than 10 mm/a, to the south, along the Java Trench, and less than 16 mm/a to the north, at the southern border of China. At these rates, Sundaland motion is compatible with the kinematics of its boundaries with the Indian and Australian plates at Burma, Sumatra and Java trenches [13], and with the Philippine Sea plate at the Philippine Trench system [18]. The geodynamic implications for the South China block have been discussed elsewhere [14]. Among the three kinematic solutions referred to in the introduction, only the one proposed by Holt et al. [1] is compatible with the minimum estimate of 16 mm/a ENE Sundaland motion. Slower motion of the South China block would imply sinistral shearing between Sundaland and South China, opposite to what is observed along the Red River fault and along the southern coast of China [14].

The possible causes for the eastward motion of Sundaland have been discussed by Le Pichon et al. [14]. To the west, the block is bounded by a dextral strike-slip zone that extends for more than 2500 km from Sunda Strait up to Burma (the GSF, the Andaman spreading system, the Sagaing Fault in Myanmar). To the south, the Java subduction evolves laterally from free subduction to collision with Australia. To the east, Sundaland is bordered by the Manilla–Philippine Trench system, over a distance of 2500 km from New Guinea to the south to Taiwan to the north. Finally to the north, the boundary with the South China block may be the southern Red River Fault and the complex system of right-lateral faulting along the coast of South China. A possibility is that Sundaland is forced to move eastward to follow the motion of the South China block. This would be compatible with right lateral shear between the two blocks. However, the size of the South China block is relatively small compared to the length of the GSF-Sagaing system to the west and the Philippine Trench system to the east, and it is unlikely that these have no effect in the force balance. Since Sundaland is pinned at its southeastern end by the collision with Australia, the clockwise rotation and eastward motion of the block may be the combined effect of right lateral shear on the GSF, right lateral shear again at the boundary with the South China block, and finally eastward escape toward the trenches on the western border of the Philippine Sea.

Acknowledgements

This paper is a contribution of the GEODYSSEA project supported by the Association of South East Asian Nations (ASEAN) and the European Commission (EC) and led by Peter Wilson [9]. We are grateful to our GEODYSSEA colleagues for providing us with pre-prints of their papers on related topics, in particular Olivier Bellier (Orsay, France), Gero Michel (GFZ, Postdam) and Wim Simons (DEOS, Delft). Eric Calais, Jeff Freymueller and Gilles Peltzer provided valuable critics on the early version of this paper, and their contribution to the final version is greatly acknowledged. Figures were prepared with GMT software [41]. ***[AC]***

References

[1] W.E. Holt, M. Li, A.J. Haines, Earthquakes strain rates and instantaneous relative motions within central and eastern Asia, Geophys. J. Int. 122 (1995) 569–593.

[2] G. Peltzer, F. Saucier, Present-day kinematics of Asia derived from geological fault rates, J. Geophys. Res. 101 (B12) (1996) 27943–27956.

[3] P. England, P. Molnar, The field of crustal velocity in Asia calculated from quaternary rates of slip on faults, Geophys. J. Int. 130 (1997) 551–582.

[4] P. England, P. Molnar, Active deformation of Asia: from kinematics to dynamics, Science 278 (1997) 647–650.

[5] T. Kato, Y. Kotake, S. Nakao, J. Beavan, K. Hirahara, M. Okada, M. Hoshiba, O. Kamigaichi, R.B. Feir, P.H. Park, M. Gerasimenko, M. Kasahara, Initial results from WING, the continuous GPS network in the western Pacific area, Geophys. Res. Lett. 25 (1998) 369–372.

[6] S.B. Yu, L.-C. Kuo, R.S. Punongbayan, E.G. Ramos, GPS observation of crustal deformation in the Taiwan–Luzon region, Geophys. Res. Lett. 26 (1999) 923–926.

[7] K. Heki, S. Miyazaki, H. Takahashi, M. Kasahara, F. Kimata, S. Miura, N.F. Vasilenko, A. Ivashchenko, The Amurian plate motion and current plate kinematics in Eastern Asia, J. Geophys. Res. (submitted).

[8] B.A.C. Ambrosius, D. Angerman, M. Becker, P. Neumaier, R. Noomen, W.J.F. Simons, C. Vigny, A. Walpersdorf, P. Wilson, Final geodetic results of the GEODYSSEA Project: the combination solution, in: American Geophysical Union, 1997 fall meeting 78, American Geophysical Union, San Francisco, CA, 1997, p. 169.

[9] P. Wilson, J. Rais, C. Reigber, E. Reinhart, A.C. Ambrosius, X. Le Pichon, M. Kasser, P. Suharto, A. Majid, P. Awang, H. Othman, B.H. Yaakub, R. Almeda, C. Boonphakdee, Study provides data on active plate tectonics in Southeast Asia Region, Eos Trans. AGU 79 (45) (1998) 545–549.

[10] W.J.F. Simons, B.A.C. Ambrosius, R. Noomen, D. Angermann, P. Wilson, M. Becker, E. Reinhart, A. Walpersdorf, C. Vigny, Observing plate motions in S.E. Asia: geodetic results of the GEODYSSEA project, Geophys. Res. Lett. (in press).

[11] A. Walpersdorf, L'observation de la tectonique active en Asie du sud-est par géodésie spatiale: un projet GPS, unpublished thesis, Univ. Paris VII, 1997.

[12] N. Chamot-Rooke, C. Vigny, W. Walpersdorf, X. Le Pichon, P. Huchon, C. Rangin, Sundaland motion detected from GEODYSSEA GPS measurements: implications for motion at Sunda trenches, in: American Geophysical Union, 1997 fall meeting 78, American Geophysical Union, San Francisco, CA, 1997, p. 169.

[13] N. Chamot-Rooke, X. Le Pichon, C. Rangin, P. Huchon, M. Pubellier, C. Vigny, A. Walpersdorf, Sundaland motion in a global reference frame detected from Geodyssea GPS measurements: Part 1. Implications for subduction motion along Java, Sumatra and Burma trenches, Geophys. J. Int. (submitted).

[14] X. Le Pichon, N. Chamot-Rooke, C. Rangin, M. Pubellier, P. Huchon, C. Vigny, A. Walpersdorf, Sundaland motion in a global reference frame detected from Geodyssea GPS measurements: Part II. Implications for motion with respect to the South China block, Geophys. J. Int. (submitted).

[15] K.L. Feigl, D.C. Agnew, Y. Bock, D. Dong, A. Donnellan, B.H. Hager, T.A. Herring, D.D. Jackson, T.H. Jordan, R.W. King, S. Larsen, K.M. Larson, M.H. Murray, Z. Shen, F.H. Webb, Space geodetic measurement of crustal deformation in Central and Southern California, 1984–1992, J. Geophys. Res. 98 (12) (1993) 21677–21712.

[16] Y. Bock, S. Wdowinski, P. Fang, J. Zhang, S. Williams, H. Johnson, J. Behr, J. Genrich, J. Dean, M. van Domselaar, D. Agnew, F. Wyatt, K. Stark, B. Oral, K. Hudnut, R. King, T. Herring, S. Dinardo, W. Young, D. Jackson, W. Gurtner, Southern California Permanent GPS Geodetic Array: Continuous measurements of regional crustal deformation between the 1992 Landers and 1994 Northridge earthquakes, J. Geophys. Res. 102 (8) (1997) 18013–18033.

[17] L. Prawirodirdjo, Y. Bock, R. McCaffrey, J. Genrich, E. Calais, C. Stevens, S.S.O. Puntodewo, C. Subarya, J. Rais, P. Zwick, Fauzi, Geodetic observations of interseismic strain segmentation at the Sumatra subduction zone, Geophys. Res. Lett. 24 (21) (1997) 2601–2604.

[18] C. Rangin, X. Le Pichon, S. Mazzotti, M. Pubellier, N. Chamot-Rooke, M. Aurelio, A. Walpersdorf, R. Quebral, Plate convergence measured by GPS across the Sundaland/Philippine Sea Plate deformed boundary: Philippines and eastern Indonesia, Geophys. J. Int. (in press).

[19] K.R. Newcomb, W.R. McCann, Seismic history and seismotectonics of the Sunda Arc, J. Geophys. Res. 92 (1987) 421–439.

[20] C.H. Scholz, J. Campos, On the mechanism of seismic decoupling and back-arc spreading at subduction zones, J. Geophys. Res. 100 (1995) 22103–22115.

[21] P. Tregoning, F.K. Brunner, Y. Bock, S.S.O. Puntodewo, R. McCaffrey, J.F. Genrich, E. Calais, J. Rais, C. Subarya, First geodetic measurement of convergence across the Java Trench, Geophys. Res. Lett. 21 (19) (1994) 2135–2138.

[22] J.C. Savage, A dislocation model of strain accumulation and release at a subduction zone, J. Geophys. Res. 88 (1983) 4984–4996.

[23] J.F. Genrich, Y. Bock, R. McCaffrey, E. Calais, C.W. Stevens, C. Subarya, Accretion of the southern Banda Arc to the Australian Plate margin determined by Global Positioning System measurements, Tectonics 15 (2) (1996) 288–295.

[24] T. Shibutani, T. Ohkura, Y. Iio et al., Search for the buried subfaults of the 16 July 1990 Luzon earthquake, the Philippines, using afterschock observations, J. Nat. Disaster Sci. 13 (1991) 29–38.

[25] J.C. Savage, R.O. Burford, Geodetic determination of relative plate motion in Central California, J. Geophys. Res. 78 (1973) 832–845.

[26] T. Duquesnoy, E. Barrier, M. Kasser, M. Aurelio, R. Gaulon, R.S. Punongbayan, C. Rangin, B.C. Bautista, E. Delacruz, M. Isada, S. Marc, J. Puertollano, A. Ramos, M. Prevot, M. Dupio, I. Eto, F.G. Sajona, D. Rigor, F.G.

Delfin, D. Layugan, Detection of creep along the Philippine Fault; first results of geodetic measurements on Leyte Island, central Philippine, Geophys. Res. Lett. 21 (11) (1994) 975–978.

[27] T. Duquesnoy, Contribution de la géodésie à l'étude de grands décrochements actifs associés à des zones de subduction à convergence oblique: exemples de la grande faille de Sumatra et de la faille Philippine, unpublished thesis, Univ. Paris Sud Orsay, 1997.

[28] M. Diament, H. Harjono, K. Karta, C. Deplus, D. Dahrin, M.T. Zen Jr., M. Gerard, O. Lassal, A. Martin, J. Malod, Mentawai fault zone off Sumatra: a new key to the geodynamics of western Indonesia, Geology 20 (3) (1992) 259–262.

[29] O. Bellier, M. Sébrier, Is the slip rate variation on the Great Sumatran Fault accommodated by fore-arc stretching?, Geophys. Res. Lett. 22 (1995) 1969–1972.

[30] T. Seno, S. Stein, A.E. Gripp, A model for the motion of the Philippine Sea Plate consistent with Nuvel I and geological data, J. Geophys. Res. 98 (1993) 17941–17948.

[31] C. DeMets, R.G. Gordon, D.F. Argus, S. Stein, Current plate motions, Geophys. J. Int. 101 (1990) 425–478.

[32] C. DeMets, R.G. Gordon, D.F. Argus, S. Stein, Effects of recent revisions to the geomagnetic reversal time scale on estimates of current plate motions, Geophys. Res. Lett. 21 (1994) 2191–2194.

[33] T. Kato, Y. Kotake, T. Chachin, Y. Iimura, S. Miyazaki, T. Kanazawa, K. Suyehiro, An estimate of the Philippine Sea Plate motion derived from the Global Positioning System observation at Okino Torishima, Japan, J. Geod. Soc. Jpn. 42 (1996) 223–243.

[34] R. McCaffrey, Global variability in subduction thrust zone–forearc systems, Pure Appl. Geophys. 142 (1) (1994) 173–224.

[35] S. Stein, R.G. Gordon, Statistical tests of additional plate boundaries from plate motion inversions, Earth Planet. Sci. Lett. 69 (1984) 401–412.

[36] R.G. Gordon, C. DeMets, D.F. Argus, Kinematic constraints on distributed lithospheric deformation in the Equatorial Indian Ocean from present motion between the Australian and Indian plates, Tectonics 9 (1990) 409–422.

[37] R. McCaffrey, Slip vectors and stretching of the Sumatran fore arc, Geology 19 (1991) 881–884.

[38] A. Tarantola, Inverse Problem Theory, Methods for Data Fitting and Model Parameters Estimation, Elsevier, Amsterdam, 1987, 613 pp.

[39] C. Frohlich, S.D. Davis, How well constrained are well-constrained T, B, and P axes in moment tensor catalogs, J. Geophys. Res. 104 (1999) 4901–4910.

[40] K.M. Larson, J.T. Freymueller, S. Philipsen, Global plate velocities from the Global Positioning System, J. Geophys. Res. 102 (5) (1997) 9961–9981.

[41] P. Wessel, W.H.F. Smith, Free software helps map and display data, Eos Trans. AGU 72 (1991) 445–446.